IEEE Transactions on Power Electronics (Early Access)

ESR Modelling of Class II MLCC Large-Signal-Excitation Losses

D. Menzi,
S. Ben-Yaakov,
G. Zulauf,
J. W. Kolar

ESR Modelling of Class II MLCC Large-Signal-Excitation Losses

David Menzi, *Member, IEEE,* Shmuel Ben-Yaakov, *Fellow, IEEE*
Grayson Zulauf, *Member, IEEE,* Johann W. Kolar, *Fellow, IEEE*

***Abstract*—Multilayer Ceramic Capacitors (MLCCs) with ferroelectric Class II dielectrics enable extremely high volumetric capacitance density, and are therefore preferred in high-power-density power conversion. These MLCCs, though, suffer from a non-linear dielectric constant and substantial low-frequency, large-signal excitation losses. Previously, a Steinmetz-parameter-based loss model accurately described these large-signal losses in MLCCs, but a difficult peak-charge measurement was required.**

For magnetic materials, a Steinmetz-based model is translated to an operating-point-specific Effective Series Resistance (ESR) model, which then allows for a low-complexity loss calculation. In this Letter, we introduce and verify an Effective Series Resistance (ESR)-based loss model for MLCCs, with the ESR derived from the MLCC Steinmetz parameters. Our modelling error is below 25 % across all evaluated operating points, a major improvement over modelling with the small-signal ESR provided in the MLCC datasheet, which may result in a loss approximation error of up to 10×.

***Index Terms*—Multilayer ceramic capacitor, MLCC, loss modelling, ESR, Steinmetz Equation, iGSE, iGSE-C, DC-AC power converters, AC-DC power converters, inverters, rectifiers, power capacitors.**

I. Introduction

Class II ferroelectric Multilayer Ceramic Capacitors (MLCCs) feature a high (relative) dielectric constant, enabling extremely high volumetric capacitance density [1]–[3] and making them the preferred capacitor technology for ultra-compact power converter systems [4,5]. These Class II MLCCs, though, exhibit non-linear dielectric constants (as shown in **Fig. 1**) and suffer from losses from low-frequency, large-signal excitations [6]–[8] that result in lower converter efficiency and may cause fatal MLCC overheating. Accurately modelling these losses, therefore, is critically important for both optimization and reliability in power converter design.

Existing loss models for Class II MLCCs under large-signal excitations suffer from the shortcomings traditional with loss modelling for non-linear passive components, including lack of extensibility, the need for difficult and time-consuming measurements, and lack of accuracy. More specifically, existing loss models can be categorized as:

- **Lookup tables** [7,8] that provide measured losses for a set of operating points (e.g., for different dc-bias and ac voltage amplitude values). These lookup tables support interpolation to predict expected MLCC losses but cannot be applied across different voltage waveforms.
- **Equivalent Series Resistance (ESR)-** or **loss-tangent-based models** [6] are widely used in the industry since they allow a straightforward loss calculation based on the excitation RMS current and/or voltage that can be easily measured. The ESR data typically available in the MLCC datasheet, though, does not accurately describe the loss behavior of Class II MLCCs under large-signal excitation [9]–[11], and a large set of measurement-based ESR values is required (similar to a loss-map-based approach) for an accurate loss calculation.
- **Steinmetz-based models** [12,13] based on the power-law relationship between MLCC losses and peak charge excitation allow an accurate loss calculation for various voltage and current waveforms but are not straightforward to apply in practice as the (non-linear) MLCC charge is not trivial to assess.

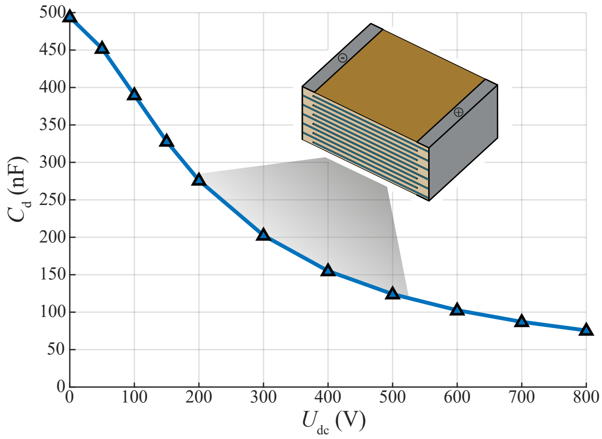

Fig. 1. Small-signal / differential capacitance C_d over dc-bias voltage U_dc of a 1 kV / 470 nF MLCC (2220Y1K00474KETWS2).

For ferromagnetic transformer core materials, Steinmetz-based loss models [14] are widely-used. There, aiming at a straightforward loss calculation, operating-point-specific ESR values are derived from the Steinmetz parameters [15,16]. Considering that the ESR model is probably the most desirable modelling approach, research is needed to explore the ferroelectric Class II MLCC losses in terms of operating-point-specific ESR values, preferably by linking the ESR values to an already proven loss model.

In this Letter, we transform the Steinmetz-based loss models [12,13] to an operating-point-specific ESR model for MLCCs, building on the proposal for this method in [17]: We show that for typical large-signal excitation voltage waveforms, the RMS value of the measured (non-sinusoidal) MLCC current and the RMS value of a sinusoidal peak-charge-equivalent current are sufficiently close such that operating-point-specific MLCC ESR values can be derived based upon the MLCC Steinmetz parameters available in literature [12,13]. Thereby, the advantages of an ESR model (i.e., a straight forward loss calculation based on the measured RMS current) and of a peak-charge-based Steinmetz model (i.e., an accurate loss calculation) are combined, accordingly simplifying the accurate MLCC loss calculation substantially.

This article has been accepted for publication in IEEE Transactions on Power Electronics. This is the author's version which has not been fully edited and
content may change prior to final publication. Citation information: DOI 10.1109/TPEL.2023.3246095

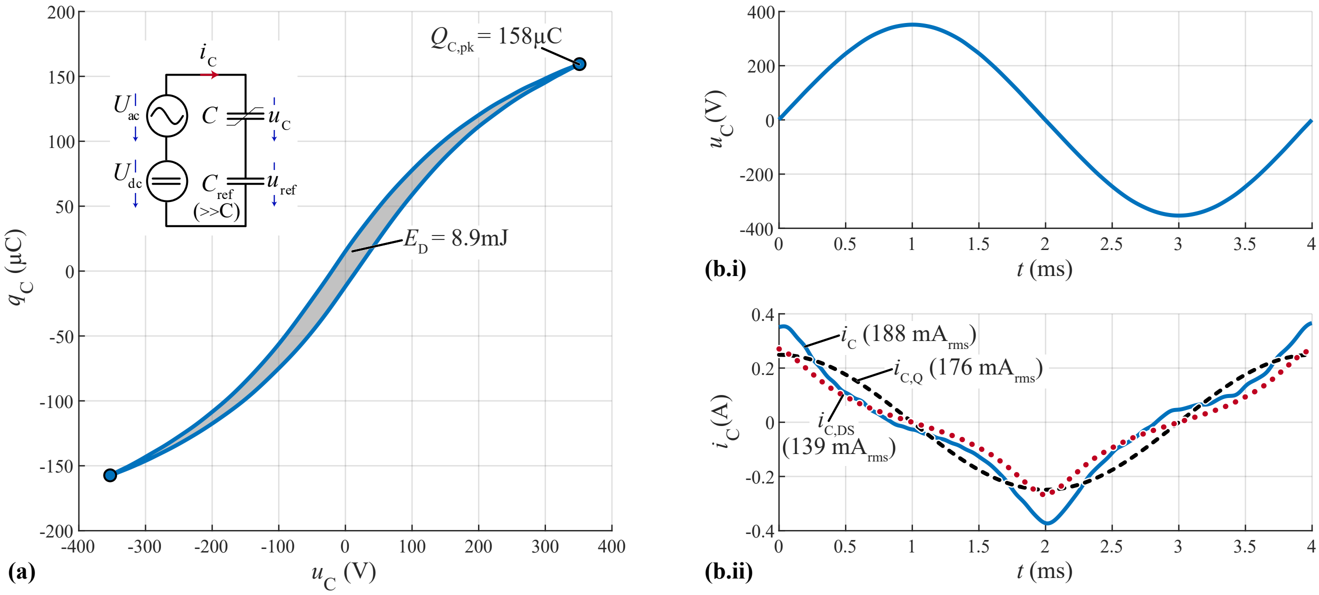

Fig. 2. **(a)** Measured voltage-charge ($U_{\rm C} - Q_{\rm C}$) hysteresis (and employed Sawyer-Tower measurement setup [12]) and **(b)** corresponding time-domain waveforms of voltage $u_{\rm C}$ **(b.i)** and current $i_{\rm C}$ **(b.ii)** of a 1 kV / 470 nF MLCC (2220Y1K00474KETWS2) excited with $U_{\rm ac} = 270\,{\rm V_{rms}}$ at f =250 Hz. The hysteresis area in **(a)** represents the dissipated energy $E_{\rm D}$ within an ac cycle and corresponds to an average power loss of 2.2 W. For comparison, **(b.ii)** also shows the peak-charge equivalent sinusoidal current $i_{\rm C,Q}$ ($I_{\rm C,Q}$ =176 mA$_{\rm rms}$), the measured, non-sinusoidal MLCC current $i_{\rm C}$ ($I_{\rm C}$ =188 mA$_{\rm rms}$), and the current $i_{\rm C,DS}$ ($I_{\rm C,DS}$ =139 mA$_{\rm rms}$) calculated from the small-signal differential capacitance of **Fig. 1**.

This Letter is structured as follows: In **Section II**, we derive the Steinmetz-based ESR model for MLCCs, and validate the model with experimental measurements in **Section III**. **Section IV** utilizes the proposed model for the design example of a 3 kW motor drive inverter, and the Letter is concluded in **Section V**.

II. Steinmetz-Based ESR Derivation

The losses in a Class II ferroelectric MLCC can be depicted with the voltage-charge ($U_{\rm C} - Q_{\rm C}$) hysteresis loop, which is shown in **Fig. 2a** for the capacitor C under test, (Knowles Syfer 2220Y1K00474KETWS2 with 1 kV / 470 nF).

The energy dissipated during one charge-discharge cycle $E_{\rm D}$ is defined by the area enclosed by the ($U_{\rm C} - Q_{\rm C}$) hysteresis loop. These MLCC large-signal excitation losses P were shown in [12,13] to fit a power law with the peak-charge excitation $Q_{\rm C,pk}$ as:

$$P = k \cdot f^{\alpha} \cdot Q_{\rm C,pk}^{\beta}, \tag{1}$$

with frequency f and the Steinmetz parameters from [12] with $k = 1.06 \cdot 10^6$, $\alpha = 1.0$, and $\beta = 2.12$ (for this capacitor).

While accurate, this Steinmetz model suffers from the disadvantage that the MLCC charge $Q_{\rm C,pk}$ is not easy to measure, as the capacitance may depend on the large-signal excitation and operating point. As we discussed in **Section I**, an ESR-based model would be preferred since the MLCC RMS current $I_{\rm C}$ is straightforward to measure. A single ESR value, though, cannot capture the non-linear loss behavior of a ferroelectric Class II MLCC [10,11], and the model must be extended.

As used in magnetic material loss modelling [16], the ESR can be derived from the Steinmetz parameters for a given operating point. The derivation of this operating-point-specific ESR value is based on an approximation of the non-linear and non-sinusoidal MLCC current $i_{\rm C}$ by means of a sinusoidal-peak-charge-equivalent current $i_{\rm C,Q}$ (peak charge is denoted as $Q_{\rm C,pk}$) with an RMS value:

$$I_{\rm C,Q} = \sqrt{2} \cdot \pi \cdot f \cdot Q_{\rm C,pk} \cdot \approx I_{\rm C}. \tag{2}$$

This RMS current corresponds to capacitor losses P based on ESR as:

$$P = ESR \cdot I_{\rm C}^2 \approx ESR \cdot I_{\rm C,Q}^2. \tag{3}$$

Alternatively, the losses P obtained from the peak-charge-based Steinmetz model (1) can be translated with (2) into

$$P = k_{\rm Q} \cdot f^{\alpha-\beta} \cdot \frac{I_{\rm C,Q}^{\beta}}{(\sqrt{2}\pi)^{\beta}} \approx k_{\rm Q} \cdot f^{\alpha-\beta} \cdot \frac{I_{\rm C}^{\beta}}{(\sqrt{2}\pi)^{\beta}}. \tag{4}$$

And, therefore, the operating-point-dependent ESR value can be calculated from the Steinmetz parameters and the measured RMS MLCC current $I_{\rm C}$ with (3) and (4) as:

$$ESR = k_{\rm Q} \cdot f^{\alpha-\beta} \cdot \frac{I_{\rm C}^{\beta-2}}{(\sqrt{2}\pi)^{\beta}}. \tag{5}$$

This equation relies on the sinusoidal current assumption, as mentioned, and the assumption that the linear MLCC peak charge $Q_{\rm C,pk}$ to RMS current $I_{\rm C}$ ratio (2) holds, which is investigated in the next section.

III. Experimental Verification

The proposed model depends upon the time-domain voltage and current measurements of the MLCC, which are shown in **Fig. 2b**. The employed Sawyer-Tower [18,19] test setup to measure the MLCC voltage $u_{\rm C}$ and charge $q_{\rm C}$ is shown in **Fig. 2a** and the MLCC current $i_{\rm C}$ is measured with a current

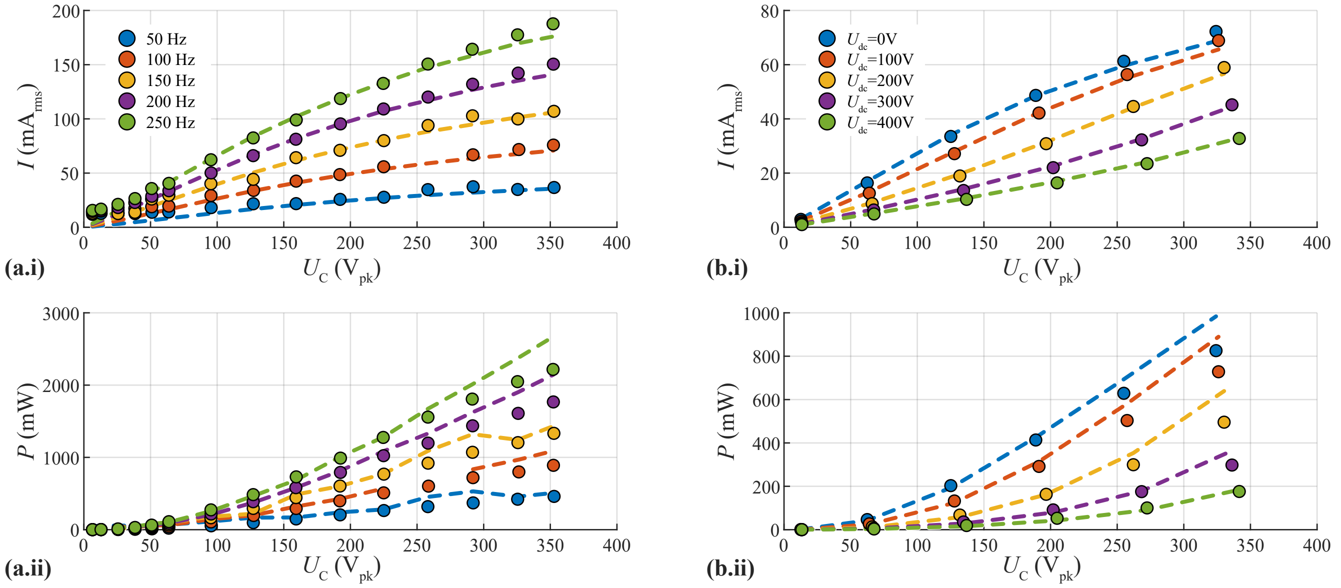

Fig. 3. Experimental data for a 1 kV / 470 nF MLCC (2220Y1K00474KETWS2) to investigate the impact of **(a)** excitation voltage amplitude $\hat{U}_{\mathrm{C}}$ and frequency f (dc bias is kept constant at $U_{\mathrm{dc}} = 0\,\mathrm{V}$), and **(b)** voltage amplitude $\hat{U}_{\mathrm{C}}$ and dc bias voltage U_{dc} (for a fixed frequency $f = 100\,\mathrm{Hz}$) on **(a.i,b.i)** the MLCC RMS current stresses I_{C} and **(a.ii,b.ii)** the power MLCC losses P. In **(a.i,b.i)**, the scatter points represent the measured RMS current I_{C} and the dashed lines represent the calculated MLCC current $I_{\mathrm{C,Q}}$ based on the measured peak charge $Q_{\mathrm{C,pk}}$ and (2). In **(a.ii,b.ii)**, the scatter points represent the measured losses and the dashed lines represent the calculated losses based on the measured RMS current I_{C} and the operating-point-specific ESR value according to (5) with the Steinmetz parameters $k = 1.06 \cdot 10^6$, $\alpha = 1.0$, and $\beta = 2.12$.

clamp. Note that the reference capacitor C_{ref} is linear such that the charge of the device under test C is defined by $q_{\mathrm{C}} = q_{\mathrm{ref}} = u_{\mathrm{ref}} \cdot C_{\mathrm{ref}}$. Here, C_{ref} acts as a capacitive shunt and it is hence important to select a low-loss (e.g., with a C0G dielectric) capacitor for the realization of C_{ref} (more details on the setup are provided in [12]).

The time-domain waveforms of **Fig. 2b** correspond to the $U_{\mathrm{C}}{-}Q_{\mathrm{C}}$ hysteresis loop in **Fig. 2a**. There, $i_{\mathrm{C,Q}}(t)$ represents the peak-charge-equivalent sinusoidal current (according to (2)), and the estimated RMS value $I_{\mathrm{C,Q}}$ deviates by less than 10 % from the measured current I_{C}.

For completeness, the MLCC current waveform $i_{\mathrm{C,DS}}(t)$ expected from the small-signal differential capacitance C_{d} of **Fig. 1** is:

$$i_{\mathrm{C,DS}}(t) = C_{\mathrm{d}}(u_{\mathrm{C}}) \frac{u_{\mathrm{C}}(t)}{\mathrm{d}t}. \tag{6}$$

This small-signal-predicted current is shown in **Fig. 2b**. The RMS current predicted from this value, $I_{\mathrm{C,DS}}$, differs by almost 30 % from the measured value I_{C}, as the large-signal capacitance behavior differs substantially from the small-signal behavior under dc bias. We see, then, that the MLCC RMS current I_{C} must be measured and cannot be calculated from datasheet information.

We next present measured data to validate the approximation (2) across excitation amplitude $\hat{U}_{\mathrm{C}}$, frequency f, and dc bias voltage U_{dc}. **Fig. 3a.i** shows the measured RMS current I_{C} (scatter points) and the estimated RMS current $I_{\mathrm{C,Q}}$ (dashed lines) across MLCC voltage $U_{\mathrm{C,pk}}$ for excitation frequencies up to $f = 250\,\mathrm{Hz}$. The deviation remains below 10 % for the full excitation voltage range across frequency. Because this deviation is minimal, the measured power losses P (**Fig. 3a.ii**, scatter points) closely match the calculated losses according to (3) and (4) (dashed lines), with a deviation below 25 % for every operating point.

It should be noted that at high excitation voltage and frequency values (i.e., higher current) there is an increase in the deviation between the measured RMS current I_{C} and the estimated RMS current $I_{\mathrm{C,Q}}$ in **Fig. 3a.i**, as well as between the measured losses and the ESR-model calculated losses in **Fig. 3a.ii**. Furthermore, the errors in the two cases are in the opposite direction. This can be explained by the fact that the employed ESR value (5) bases on $Q_{\mathrm{C,pk}}$ and the charge-equivalent current $I_{\mathrm{C,Q}}$: The deviation between the measured I_{C} and the estimated $I_{\mathrm{C,Q}}$ increases with the current magnitude (I_{C} is larger than $I_{\mathrm{C,Q}}$, see **Fig. 3a.i**), and hence, the calculated losses according to (4) over estimate the measured power loss in **Fig. 3a.ii**. This error could possibly be reduced by directly conducting a Steinmetz fit on the measured losses and the RMS MLCC current I_{C}, which is intended to be done in a follow up study.

Similarly, the impact of DC bias on the model is evaluated in **Fig. 3b** (for an excitation frequency $f = 100\,\mathrm{Hz}$). Across the full excitation voltage, again, the RMS current and loss estimation errors remains below 5 % and 25 %, respectively.

Therefore, the proposed model – an ESR model based upon the peak-charge based Steinmetz parameters – accurately predicts large-signal MLCC losses from measured current. The improved accuracy of the model is especially stark when compared to a model that utilizes the small-signal ESR value from the datasheet, which can result in an error of up to a factor of ten [12].

IV. Design Example

We apply the proposed – and now validated – model to a practical design example, shown in **Fig. 4**. Here, MLCCs are used in a full-sinewave filter with a capacitance $C_{\mathrm{f}} = 1.2\,\mathrm{\mu F}$

for a 3 kW motor drive inverter. This sinewave filter is designed to limit the high-frequency motor stresses of an induction machine (Siemens 1LE1003-1AA42-2NA4-Z H01, $U_{\mathrm{ac}} = 230\,\mathrm{V_{rms}}$ line-to-neutral voltage, $f = 100\,\mathrm{Hz}$ nominal stator frequency, 5820 rpm nominal speed). The inverter operates with a dc-link voltage U_{in} =800 V and the filter capacitors are referenced to the positive C_{f1} and negative C_{f2} dc-link rail to provide both common- and differential-mode attenuation and to reduce the overall capacitance variation [20,21].

During operation, both C_{f1} and C_{f2} are subject to a dc bias of $U_{\mathrm{dc}} = U_{\mathrm{in}}/2$=400 V and peak voltages up to $U_{\mathrm{Cf1,max}} = U_{\mathrm{Cf2,max}} = U_{\mathrm{in}} + \hat{U}_{\mathrm{ac}}$ =725 $\mathrm{V_{pk}}$. At this operating point, the minimum capacitance values of C_{f1} and C_{f2} drop as low as 17 % of the nominal capacitance value (see **Fig. 1**), but the filter structure limits the non-linearity of the effective capacitance value $C_{\mathrm{f}} = C_{\mathrm{f1}}+C_{\mathrm{f2}}$ to 32 % (with the minimum value occurring at the voltage zero crossing in a motor ac period). Therefore, to achieve a minimum capacitance value $C_{\mathrm{f}} = 1.2\,\mu\mathrm{F}$, a total of eight 470 nF MLCCs (i.e., four devices each referenced to the positive and negative dc-link rail) is required.

In the test setup (see **Fig. 2a**) a single MLCC is exposed to the nominal operating point condition for the considered application, i.e., excited with $\hat{U}_{\mathrm{C}}$ =325 $\mathrm{V_{pk}}$ / U_{dc} =400 V / f = 100 Hz), which results in a measured RMS current of I_{C} =33 $\mathrm{mA_{rms}}$. With this measurement, we can calculate the ESR according to (5) as 171 Ω and calculate per-capacitor losses of 184 mW. Under this same large-signal excitation, the losses are directly measured with the Sawyer-Tower circuit as 176 mW, and the proposed model accurately predicts the losses to within 5 % of the measurement. The total filter capacitor losses are 1.5 W per inverter phase and 4.4 W total for the inverter sinewave filter.

Note that the employed Steinmetz parameters were recorded at room temperature (25 °C) while the MLCC losses will cause self-heating above ambient temperature. However, the MLCC losses were found to decrease with increasing temperature by approximately 0.6 %/K in [12], so the design approach is conservative and thermal runaway can be ruled out. According to [6], up to 900 mW can be dissipated for the particular MLCC without a temperature increase above 20 °C, so there is sufficient margin for modelling inaccuracies and the MLCC switching-/high-frequency losses (see e.g., [22,23]), which are typically small compared to the low-frequency large-signal excitation losses in a sinewave filter [12] and hence not considered here.

In some other practical applications, there might be a need to connect capacitors in parallel for handling higher current, and/or in series to handle higher voltages. In case of a parallel connection, the MLCC current excitation is directly defined by the large-signal voltage excitation and the losses can be calculated independently for each device. In the case several devices are connected in series the excitation voltage will be shared – as a first approximation – according to the impedance ratio of the MLCCs, where balancing resistors are required to assure equal dc voltage sharing. Here, the measured RMS current flowing through the series connection of the MLCCs can of course be employed to calculate the MLCC losses of each device.

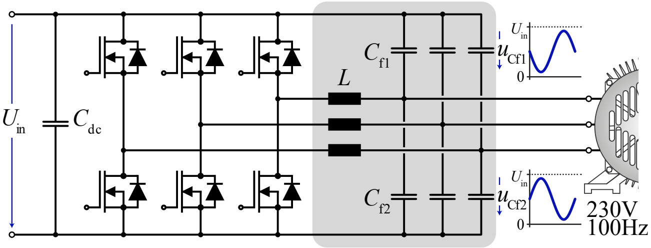

Fig. 4. Design example: inverter sinewave output filter to reduces the high-frequency stresses of a 230 $\mathrm{V_{rms}}$/100 Hz three-phase machine, with positive C_{f1} and negative C_{f2} dc-link-referenced filter capacitors [20,21].

V. Conclusion

Multilayer Ceramic Capacitors (MLCCs) with ferroelectric Class II dielectrics enable extremely high volumetric capacitance density – and therefore power-dense power converters – but these capacitors suffer from a non-linear dielectric constant and, in certain applications, substantial large-signal excitation losses. Our previous work introduced a peak-charge-based MLCC Steinmetz-loss model that accurately described the MLCC power losses under various large-signal operating conditions, including biased and non-sinusoidal excitation voltage waveforms, but this model suffered from the shortcoming that the MLCC peak charge is not easily measured.

In this Letter, we proposed and validated a simplified, accurate Equivalent Series Resistance (ESR)-based MLCC loss model that calculates the operating-point-specific ESR from *only* Steinmetz parameters and a current measurement, which is much more straightforward than a peak charge measurement. Even under the model assumptions, a loss error between the model and our measurements for a representative AC was below 25 % at every considered operating point which is a major improvement compared to a model that utilizes the small-signal ESR value from the datasheet, which can result in an error of up to a factor of ten. In a design example for a sine-wave filter in a 3 kW motor drive inverter, the model was demonstrated to predict losses within 5 % of the measured dissipated power.

With an accurate model and a straightforward measurement, these critical losses can be predicted across a range of applications. Steinmetz parameters for a large number of X7R and X7T Class II MLCCs are provided in [13], supporting the fast and broad adoption of the MLCC ESR-based model described in this Letter.

References

[1] M. Randall, D. Skamser, J. Kinard, and A. Tajuddin, "Thin film MLCC," in *Proc. of the Symposium for Passive Components (CARTS)*, 2007.

[2] M. J. Pan and C. Randall, "A brief introduction to ceramic capacitors," *IEEE Electrical Insulation Magazine*, vol. 26, no. 3, pp. 44–50, 2010.

[3] Knowles Syfer, "Syfer Application Notes," 2014. [Online]. Available: https://www.digikey.ee/en/pdf/k/knowles-syfer/application-notes

[4] Y. Lei, C. Barth, S. Qin, W. C. Liu, I. Moon, A. Stillwell, D. Chou, T. Foulkes, Z. Ye, Z. Liao, and R. C. Pilawa-Podgurski, "A 2-kW single-phase seven-level flying capacitor multilevel inverter with an active energy buffer," *IEEE Transactions on Power Electronics*, vol. 32, no. 11, pp. 8570–8581, 2017.

[5] D. Bortis, D. Neumayr, and J. W. Kolar, "$\eta\rho$-Pareto optimization and comparative evaluation of inverter concepts considered for the GOOGLE Little Box Challenge," *Prof. of the IEEE Workshop on Control and Modeling for Power Electronics (COMPEL)*, 2016.

[6] Johanson Dielectrics, "AC power computations for DC rated capacitors," May 2005. [Online]. Available: https://www.johansondielectrics.com/downloads/ac-power-computations-for-dc-rated-capacitors.pdf

[7] D. Neumayr, D. Bortis, J. W. Kolar, M. Koini, and J. Konrad, "Comprehensive large-signal performance analysis of ceramic capacitors for power pulsation buffers," in *Proc. of the IEEE Workshop on Control and Modeling for Power Electronics (COMPEL)*, 2016, pp. 1–8.

[8] C. B. Barth, T. Foulkes, I. Moon, Y. Lei, S. Qin, and R. C. Pilawa-Podgurski, "Experimental evaluation of capacitors for power buffering in single-phase power converters," *IEEE Transactions on Power Electronics*, vol. 34, no. 8, pp. 7887–7899, 2019.

[9] S. Ben-Yaakov, "Some observations on loss and hysteresis of ferroelectric-based ceramic capacitors," *IEEE Transactions on Power Electronics*, vol. 33, no. 11, pp. 9127–9129, 2018.

[10] L. E. Mosley, "Capacitor impedance needs for future microprocessors," in *Proc. of the Symposium for Passive Components (CARTS)*, 2006, pp. 168–178.

[11] A. Raciti, S. Rizzo, N. Salerno, G. Susinni, R. Scollo, and A. Scuto, "Modeling the hysteresis power losses of the output parasitic capacitance in super junction MOSFETs," in *Proc. of the IEEE International Symposium on Power Electronics, Electrical Drives, Automation and Motion (SPEEDAM)*, 2018, pp. 527–532.

[12] D. Menzi, D. Bortis, G. Zulauf, M. Heller, and J. W. Kolar, "Novel iGSE-C loss modelling of X7R ceramic capacitors," *Transactions on Power Electronics*, vol. 35, pp. 13 367–13 383, 2020.

[13] D. Menzi, M. Heller, and J. W. Kolar, "iGSE-Cx – A new normalized Steinmetz model for Class II multilayer ceramic capacitors," *IEEE Open Journal of Power Electronics*, vol. 2, pp. 138–144, 2021.

[14] Steinmetz, Proteus Charles, "On the law of hysteresis," *Transactions of the American Institute of Electrical Engineers*, vol. 9, no. 1, pp. 1–64, 1892.

[15] J. G. Zhu, S. Y. R. Hui, and V. S. Ramsden, "A generalized dynamic circuit model of magnetic cores for low- and high-frequency applications - Part I: Theoretical calculation of the equivalent core loss resistance," *IEEE Transactions on Power Electronics*, vol. 11, no. 2, pp. 246–250, 1996.

[16] J. Yao, Y. Li, H. Zhao, and S. Wang, "Design of CM inductor based on core loss for radiated EMI reduction in power converters," in *Proc. of the IEEE Applied Power Electronics Conference and Exposition (APEC)*, Mar. 2019, pp. 2673–2680.

[17] Sam Ben-Yaakov, "Modeling ceramic capacitors loss under high DC bias voltage and high current stress," Jun. 2022. [Online]. Available: https://www.youtube.com/watch?v=d00FQxDmWCI

[18] C. B. Sawyer; C. H. Tower, "Rochelle salt as a dielectric," *PHYSICAL REVIEW*, pp. 732–732, 1929.

[19] E. A. Pecherskaya, "The use of the Sawyer-Tower method and its modifications to measure the electrical parameters of ferroelectric materials," *Measurement Techniques*, vol. 50, no. 10, pp. 1101–1107, Oct. 2007.

[20] F. Maislinger, H. Ertl, G. Stojcic, and L. Siplika, "Performance of a two-stage actively damped LC Filter for GaN/SiC motor inverters," in *Proc. of the IEEE International Conference on Power Electronics and Motion Control (PEMC)*, 2018, pp. 177–183.

[21] F. Maislinger, H. Ertl, G. Stojcic, C. Lagler, and F. Holzner, "Design of a 100 kHz wide bandgap inverter for motor applications with active damped sine wave filter," *The Journal of Engineering*, vol. 2019, no. 17, pp. 3766–3771, 2019.

[22] S. Coday and R. C. N. Pilawa-Podgurski, "High accuracy calorimetric measurements and modeling of ceramic capacitor losses under large ripple operation," in *Proc. of the IEEE Applied Power Electronics Conference (APEC)*, 2020, pp. 188–194.

[23] Y. Jiang, B. Hu, B. Wen, Y. Shen, and T. Long, "Methodology for large-signal loss characterization of ferroelectric Class II MLCC in high-frequency range," in *Proc. of the IEEE Energy Conversion Congress and Exposition (ECCE USA)*, 2022, p. 6.